7

Phase Unwrapping

7.1 Basic Concepts

In Chapters 5 and 6, we discussed the construction and filtering of a phase-wrapped interferogram derived from two geometrically aligned single look complex images. An example is shown in Figure 6.2 and repeated here as Figure 7.1. Each color cycle, or fringe, represents a phase change of 2π. This can be converted to a line of sight (LOS) distance change as

$$d_{LOS} = -\phi \frac{\lambda}{4\pi} \tag{7.1}$$

where ϕ is the phase change given in Equation 6.2 and λ is the wavelength of the radar (Table 7.1). Here, the LOS direction is defined as the direction of the ground toward the radar, so a minus sign is needed. In this case of a Sentinel-1 interferogram having a wavelength of 56 mm, one interferometric fringe represents –28 mm of LOS deformation.

The wrapped interferogram is colorful and shows the areas around the fault having the largest deformation, but we need to count, or unwrap, the fringes to determine the LOS deformation difference between any two points in the image. For example, we may want to know the surface rupture offset between two points **a** and **b** on either side of the fault shown in Figure 7.1 (a). One could manually count the number of fringes along the path shown by the black curve, but a computer can do this much faster and perhaps more accurately.

In this chapter we discuss the theory and algorithms used to unwrap the phase to produce a map of LOS deformation. It is often assumed that the unwrapped phase is a smooth function, analogous to an analytic function in calculus. In theory, converting the wrapped phase to the unwrapped phase is simple. All we need to do is add multiples of 2π to selected pixels to ensure that the differences between adjacent pixels are less than $|\pi|$. For high-quality data, this process can be automated

Downloaded from https://www.cambridge.org/core. UNIVERSIDAD AUTONOMA METROPOLITANA, on 13 Nov 2026 at 03:08:40, subject to the Cambridge Core terms of use, available at https://www.cambridge.org/core/terms. https://doi.org/10.1017/9781009606226.008

Table 7.1 *Radar wavelength for commonly used satellites.*

Satellite	Wavelength (λ)	Band
Sentinel-1, ERS, Envisat	56 mm	C
ALOS-1/2	236 mm	L
TerraSAR-X	31 mm	X
NISAR	93 mm and 240 mm	S and L

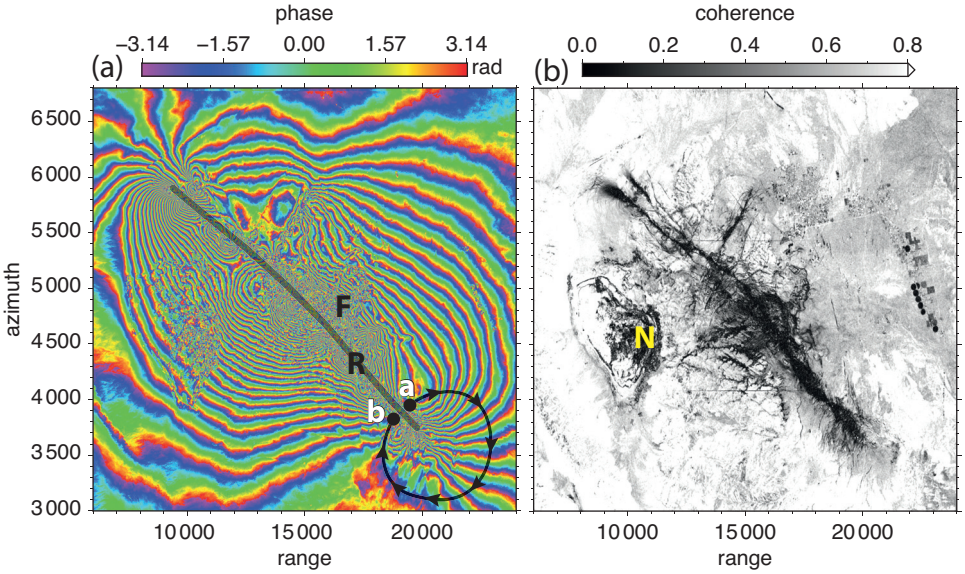


Figure 7.1 (a) Interferogram between July 4 and July 16, 2019, showing displacement due to the July 5, Ridgecrest earthquakes in radar coordinates. One fringe is 28 mm of ground deformation. Label **F** marks an area where the fringes are aliased because the rate exceeds 2π per pixel. Label **R** marks the fault rupture where the phase is discontinuous. One could count the number of fringes along the path from **a** to **b** as a measure of the offset of the surface rupture. (b) Coherence for the interferogram shows mostly high coherence away from the main ruptures. The area of low correlation along the main rupture zones and to the left of the ruptures with label **N** causes phase noise making unique unwrapping challenging.

easily (e.g., Itoh (1982)). However, for typical 2D InSAR data, this simple approach usually yields poor results because of five confounding effects:

1. phase noise due to areas of low coherence between the reference and repeat images (**N** in Figure 7.1 (b));
2. spatial aliasing in areas where the separation between fringes is smaller than the range or azimuth resolution of the filtered radar image (50 meters in this example) (**F** in Figure 7.1 (a));

Downloaded from https://www.cambridge.org/core. UNIVERSIDAD AUTONOMA METROPOLITANA, on 13 Nov 2026 at 03:08:40, subject to the Cambridge Core terms of use, available at https://www.cambridge.org/core/terms. https://doi.org/10.1017/9781009606226.008

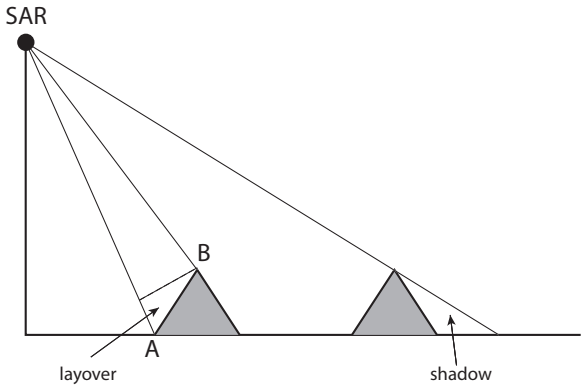


Figure 7.2 (a) Layover occurs when the range to the top of a mountain **B** is less than the range to the base of the mountain **A**; this produces discontinuous phase in an interferogram. (b) A shadow occurs when there is no radar energy reflected from the ground on the far side of the mountain; this also produces discontinuous phase in an interferogram.

3. a discontinuity in the ground displacement due to the surface rupture (**R** in Figure 7.1 (a));
4. a region of *layover* where the slope of the topography exceeds the incidence angle of the radar. In the case of Sentinel-1, the incidence angle varies from about 20° in the near range to 60° in the far range (Figure 7.2). Suppose there is a mountain having a 30° slope facing the direction of the radar in the near range of the image where the incidence angle is 20°, then the range to the top of the mountain is less than the range to the bottom of the mountain so the phase will be discontinuous;
5. similarly, if the backside of the mountain, facing away from the radar, is steeper than the incidence angle, then there will be a slope that is not illuminated by the radar (*shadow*), also resulting in discontinuous phase (Figure 7.2).

Before going into the phase unwrapping algorithms, it is instructive to review the properties of analytic functions. Let's assume we have a perfect wrapped interferogram with none of the five confounding effects discussed earlier and we want to unwrap the phase. After unwrapping the phase, it will be an analytic function of two variables x-range and y-azimuth $\mathbf{x} = (x, y)$. Consider the integration of the gradient of the phase around any closed path C containing area A. Assuming the phase is continuous, and has continuous derivatives, this closed-path integral will be zero.

$$\oint_C \nabla\phi \cdot d\mathbf{x} = 0 \tag{7.2}$$

Downloaded from https://www.cambridge.org/core. UNIVERSIDAD AUTONOMA METROPOLITANA, on 13 Nov 2026 at 03:08:40, subject to the Cambridge Core terms of use, available at https://www.cambridge.org/core/terms. https://doi.org/10.1017/9781009606226.008

Also, by Green's theorem, we have the following relationship relating the path integral of the phase gradient to the area integral of the curl of the phase gradient (Ghiglia and Pritt, 1998)

$$\oint_C \nabla\phi \cdot d\mathbf{x} = \int \int_A \left(\frac{\partial^2 \phi}{\partial x \partial y} - \frac{\partial^2 \phi}{\partial y \partial x} \right) dxdy. \tag{7.3}$$

We can shrink this area down to the resolution size of the interferogram and compute the integrand on the right side of Equation 7.3. In theory this should be zero. If it is significantly different from zero, then the path integral around that point is not zero. Goldstein et al. (1988) call this point a *residue* as an analogy to a residue from the integration of a function around a pole in the complex plane. The residue reflects a phase discontinuity of $N2\pi$ where N defines the integer unwrapping error.

We have performed these derivatives in Equation 7.3 using the phase gradients of the Sentinel-1 data (Figure 7.3 (a,b)) for the Ridgecrest earthquake and arrive at the residue maps shown in Figure 7.3 (c–f). Because of phase noise and other effects, the residue is never exactly zero. However, this analysis clearly reveals large residues, both positive and negative. For example, there is a concentration of residues along areas of surface fracture (Figure 7.3 (e)). Most of the phase unwrapping algorithms perform an analysis to first identify the residues and then avoid the residue areas during phase unwrapping.

A wide variety of algorithms have been developed to address these issues. The algorithms fall into two main categories: global and local (Ghiglia and Pritt, 1998). Local algorithms begin at a single pixel and expand outward along paths that cover the entire image, while global algorithms attempt to find an approximate solution that fits all pixels simultaneously (Ghiglia and Pritt, 1998). We first discuss a global algorithm that uses a Fourier transform approach for phase unwrapping. This and the other global methods, more completely discussed in Ghiglia and Pritt (1998), are mathematically elegant and sometimes computationally efficient, but they suffer from long-wavelength unwrapping errors caused by residues. The local algorithms are more accurate and have the special property that when the unwrapped phase is re-wrapped, the result matches the starting wrapped phase so they simply add $N2\pi$ to each pixel; these algorithms seek the integer phase ambiguity that minimizes some objective function, such as minimizing the phase gradient. We discuss the Goldstein et al. (1988) residue-cut algorithm and then the more widely used Statistical-Cost, Network-Flow Algorithm for Phase Unwrapping (SNAPHU) (Chen and Zebker, 2002). The notes later on the Goldstein and SNAPHU algorithms are derived from the excellent papers by Chen and Zebker (2000, 2001).

Downloaded from https://www.cambridge.org/core. UNIVERSIDAD AUTONOMA METROPOLITANA, on 13 Nov 2026 at 03:08:40, subject to the Cambridge Core terms of use, available at https://www.cambridge.org/core/terms. https://doi.org/10.1017/9781009606226.008

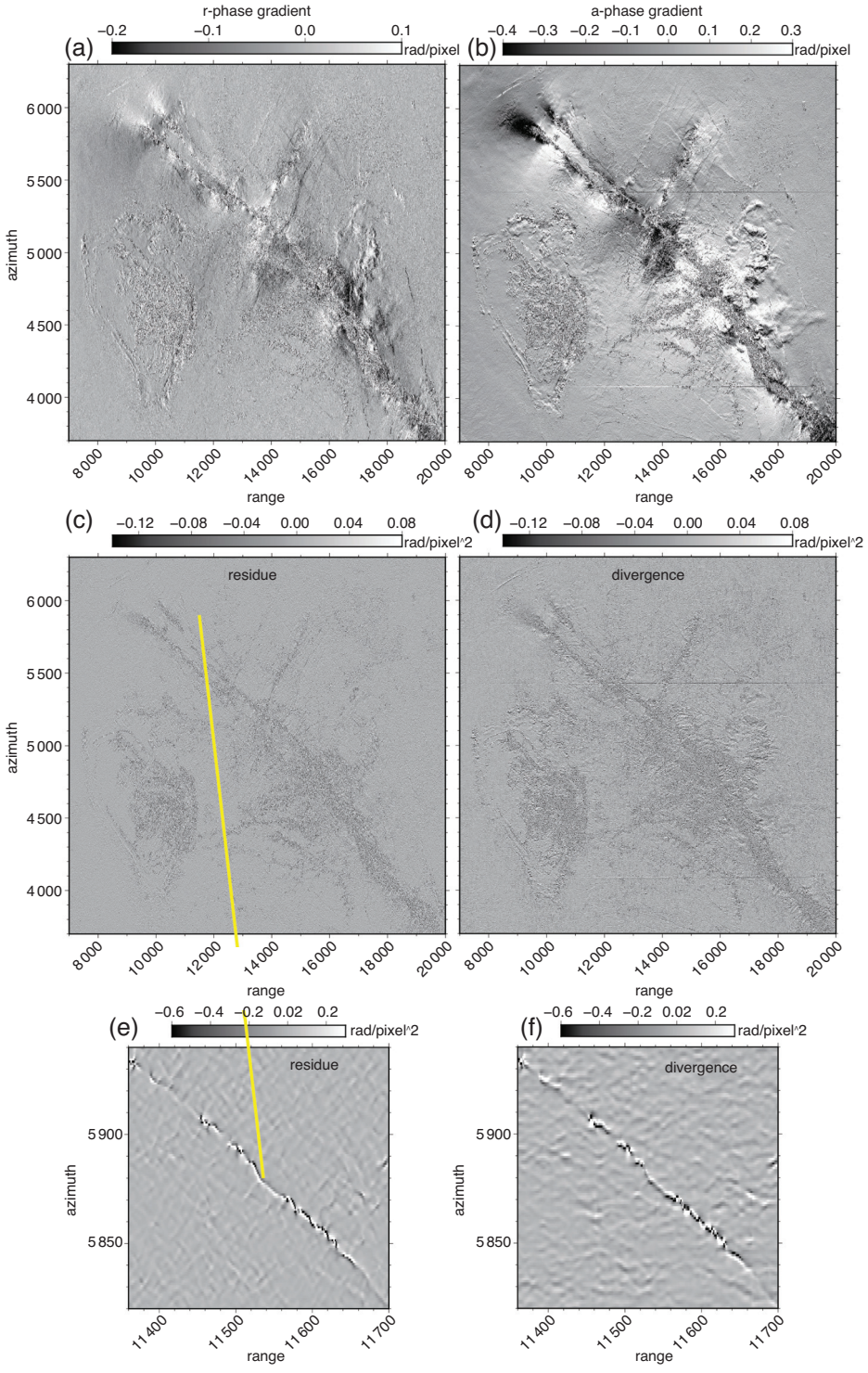


Figure 7.3 (a, b) Range and azimuth phase gradients for the Ridgecrest earthquakes. (c, e) Residue given in Equation 7.3. High residue, both positive and negative, occurs in areas of higher phase noise and surface ruptures. A zoom of a small surface rupture, having a phase offset of less than one fringe, shows a line of enhanced dipolar residue. (d, f) Divergence of the phase gradient (Equation 7.6) is used in the Fourier transform unwrapping algorithm.

Downloaded from https://www.cambridge.org/core. UNIVERSIDAD AUTONOMA METROPOLITANA, on 13 Nov 2026 at 03:08:40, subject to the Cambridge Core terms of use, available at https://www.cambridge.org/core/terms. https://doi.org/10.1017/9781009606226.008

7.2 Fourier Transform Algorithm

The first method considered is a global one that uses the Helmholtz identity, followed by a 2-D Fourier analysis, to perform the integration. Let the observed phase gradient be given by

$$\mathbf{u}(\mathbf{x}) = \left(\frac{\partial \phi}{\partial x}, \frac{\partial \phi}{\partial y}\right) = \frac{R\nabla I - I\nabla R}{R^2 + I^2} \tag{7.4}$$

where we use the real $R(\mathbf{x})$ and imaginary $I(\mathbf{x})$ parts of the interferogram to compute the gradient (i.e., Equation 6.13). Using the Helmholtz decomposition, the phase gradient vector field can be decomposed as the sum of an irrotational vector (curl-free) field and a solenoidal (divergence-free) vector field

$$\mathbf{u}(x) = -\nabla\phi + \nabla \times \psi \tag{7.5}$$

where ϕ is a scalar potential (i.e., unwrapped phase) and ψ is a vector potential. We assume that the phase is a conservative function so the rotational part of the vector field must be zero everywhere. As shown by Ghiglia and Pritt (1998), this corresponds to minimizing the integral of the square of the difference between the observed phase gradient and the recovered gradient. For real phase gradient data, the five factors described above introduce a rotational component that should be eliminated. This is accomplished by taking the divergence of Equation 7.5 since, by definition, $\nabla \cdot \nabla \times \psi = 0$. The phase and phase gradient are now related by Poisson's equation (Ghiglia and Pritt, 1998; Sandwell and Price, 1998).

$$\nabla^2\phi = -\nabla \cdot \mathbf{u} \tag{7.6}$$

For a finite region, the outward component of the phase gradient should be zero along the boundaries (Ghiglia and Romero, 1994); $\nabla\phi \cdot \mathbf{n} = 0$, where $\mathbf{n}$ is the outward normal. An example of the divergence of the phase gradient is shown in Figure 7.3 (d,f). The 2-D Fourier transform of Equation 7.6 is

$$4\pi^2\left(k_x^2 + k_y^2\right)\Phi(\mathbf{k}) = i2\pi\left[k_x U_x(\mathbf{k}) + k_y U_y(\mathbf{k})\right] \tag{7.7}$$

where $\mathbf{k} = \left(k_x, k_y\right)$ are the wavenumbers and the forward and inverse 2-D Fourier transforms of a function $f(x, y)$ are given as

$$\begin{aligned} F(\mathbf{k}) &= \int_{-\infty}^{\infty}\int_{-\infty}^{\infty} f(x,y)e^{-i2\pi\left(k_x x + k_y y\right)}dxdy = \mathcal{F}_2[f] \\ f(\mathbf{x}) &= \int_{-\infty}^{\infty}\int_{-\infty}^{\infty} F\left(k_x, k_y\right)e^{+i2\pi\left(k_x x + k_y y\right)}dk_x dk_y = \mathcal{F}_2^{-1}[F]. \end{aligned} \tag{7.8}$$

Downloaded from https://www.cambridge.org/core. UNIVERSIDAD AUTONOMA METROPOLITANA, on 13 Nov 2026 at 03:08:40, subject to the Cambridge Core terms of use, available at https://www.cambridge.org/core/terms. https://doi.org/10.1017/9781009606226.008

Solving for the total unwrapped phase, we find

$$\phi_{tot}(\mathbf{x}) = \mathcal{F}_2^{-1}\left\{\frac{i\mathbf{k}\cdot\mathcal{F}_2[\mathbf{u}]}{2\pi\left(k_x^2+k_y^2\right)}\right\}. \tag{7.9}$$

For a finite size region, the Fourier transform is replaced by a Fourier series. The zero phase-gradient boundary condition is satisfied if a 2-D cosine transform is used (Ghiglia and Romero, 1994). In practice, one takes the 2-D Fourier transform of each component of the phase gradient with a sine transform in the gradient direction and the cosine transform in the orthogonal direction. Then the result is scaled by the wavenumbers in Equation 7.9. Finally, one takes the inverse 2-D cosine transform to recover the total phase.

An example of topography derived from stacked phase gradients from ERS interferograms, combined with a 90-m Unites States Geologic Survey (USGS) reference topography, is shown in Figure 7.4 (Sandwell and Sichoix, 2000). This topography was developed so it could be removed from individual interferograms to isolate the phase caused by interseismic deformation. At that time (year 2000), the topographic phase was the largest error source in the recovery of deformation because the near-global, 30-m resolution, SRTM topography had not been collected (Farr et al., 2007).

Stacking of phase gradients increases the effective interferometric baseline, which increases the topographic signal to atmospheric noise ratio. As discussed next, the relatively low-resolution USGS reference topography is needed to minimize long-wavelength unwrapping error.

A major issue with the Fourier transform unwrapping approach is that simply removing the rotational part of the phase gradient introduces errors in areas where there are residues. In this case of topographic recovery, there is significant layover in the mountain areas, which results in long-wavelength errors in the unwrapped phase and thus errors in the recovered topography. There are three approaches to mitigating these errors. (1) One can replace the Fourier transform inversion Equation 7.6 with a weighted least-squares inversion where the weights are related to the density of the residues (Ghiglia and Pritt, 1998). The main problem with this approach is the least-squared design matrix becomes extremely large and may exceed even today's computer capabilities. Moreover, there is no guarantee that when this phase is re-wrapped, it will match the phase of the original interferogram. (2) One can use a remove–restore approach to retain the long-wavelength topography from an existing low-resolution topography model. In this case (Figure 7.4), the USGS topography was removed during the formation of each interferogram and the phase gradients were computed and stacked. After Fourier unwrapping the residual stack, the residual phase was high-pass filtered and the USGS model was

Downloaded from https://www.cambridge.org/core. UNIVERSIDAD AUTONOMA METROPOLITANA, on 13 Nov 2026 at 03:08:40, subject to the Cambridge Core terms of use, available at https://www.cambridge.org/core/terms. https://doi.org/10.1017/9781009606226.008

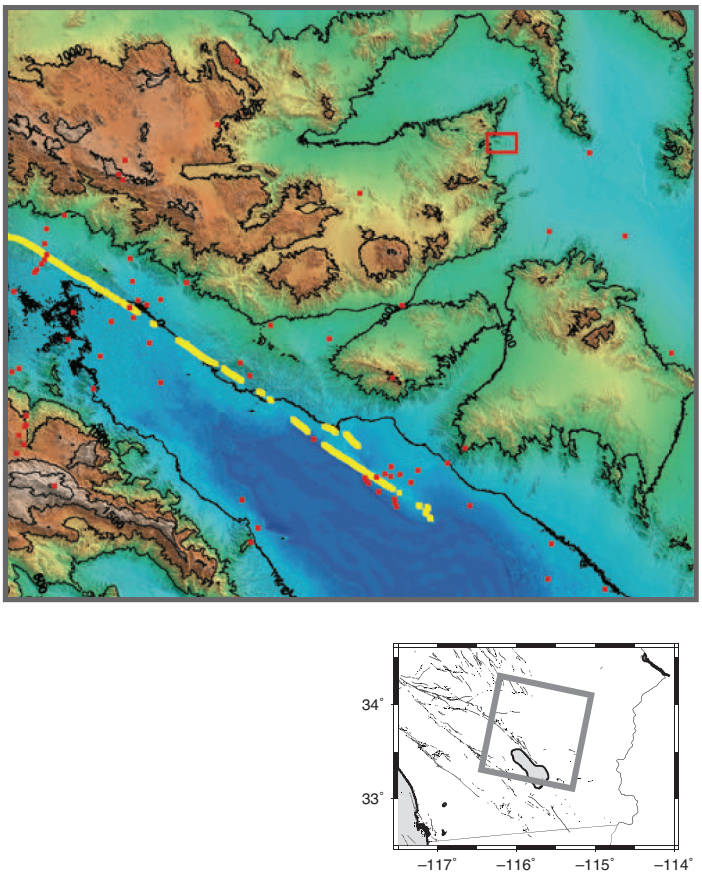


Figure 7.4 Topography (meters above WGS84 ellipsoid, 500-m contour interval, radar coordinates) of the Salton Sea area (see inset map) includes the southern segments of the San Andreas Fault (yellow) and GPS monuments (red). This image combines the long-wavelength accuracy of the USGS 90-m DEM with the short-wavelength (< 6 km) phase gradient information from a stack of 25 ERS SAR images. The combined DEM has 16-m postings and a vertical accuracy of 10 m.

restored. (3) Iterating this remove–restore approach results in a DEM having both long-wavelength accuracy and short-wavelength resolution.

The phase gradient stacking followed by Fourier unwrapping and an iterative remove–restore is a viable approach for topographic recovery. However, for measuring surface deformation, the long-wavelength errors of the Fourier transform method are not acceptable. Moreover, since the existing DEMs from the SRTM mission (Farr et al., 2007) and, more recently, the TerraSAR Tandem-X DEM (Zink et al., 2014) are available for accurate topographic phase removal, thus Fourier transform unwrapping approach is rarely used today.

Downloaded from https://www.cambridge.org/core. UNIVERSIDAD AUTONOMA METROPOLITANA, on 13 Nov 2026 at 03:08:40, subject to the Cambridge Core terms of use, available at https://www.cambridge.org/core/terms. https://doi.org/10.1017/9781009606226.008

7.3 Branch Cut (Goldstein) Algorithm

As discussed earlier, the main objective of 2-D phase unwrapping is to integrate the measured phase gradient to uniquely recover the total phase. If we start the integration at point a, then the phase at point b is the integral of the phase gradient along a path connecting the two points

$$\phi(x,y) = \int_a^b \nabla\phi \cdot d\mathbf{x} + \phi(x_a, y_a). \tag{7.10}$$

Of course, there is an unknown constant of integration $\phi(x_a, y_a)$. Assuming the true interferogram represents a continuous function such as topography, surface deformation, or atmospheric delay, the integration of the phase gradient, around any closed loop, should be zero. The occurrence of nonzero phase closure, or residue, is somewhat predictable. Images with low coherence typically contain high densities of residues, which can make unwrapping challenging. Topographic layover and shadows typically create lines of residues along the edge of the layover. Abrupt discontinuities due to surface faulting or glacier movement also generate residues. It is possible that entire regions of the interferogram may be isolated from other regions by residues and the associated branch cuts. In these cases, ad hoc assumptions (e.g., there are minimal phase jumps between isolated regions) may be necessary to ensure a reasonable result.

To identify the residues, consider a wrapped interferogram as a 2-D array of normalized phase values as shown in Figure 7.5. Because the phase is wrapped, all the values lie between 0 and 1. If the absolute value of the phase difference between two cells is greater than 0.5, then there is a phase wrap and one must add or subtract 1 to obtain stay within the 0.5 phase difference. Let's check some examples for phase closure. Consider the closure at node **A**. Summing the phase difference counterclockwise from the upper left corner, we have −.9+.8−.1+.2. The first two cell differences exceed 0.5, so we add 1 to the first and subtract 1 from the second so

closure at cell **A** is +.1 −.2 −.1 +.2 = 0
closure at cell **B** is +.1 −.1 −.2 +.2 = 0
closure at the **+** cell is +.2 +.3 +.2 +.3 = +1
closure the **–** cell is −.2 −.3 −.1 −.4 = −1

In this small grid, there are two residues with opposite signs. To confirm the residues cancel, we integrate around a loop containing both residues +.2+.3+.1−.3−.1−.4−.1+.3 = 0. Therefore, to achieve path independence with the phase gradient integration, the path cannot cross between the + and – residues. A

Downloaded from https://www.cambridge.org/core. UNIVERSIDAD AUTONOMA METROPOLITANA, on 13 Nov 2026 at 03:08:40, subject to the Cambridge Core terms of use, available at https://www.cambridge.org/core/terms. https://doi.org/10.1017/9781009606226.008

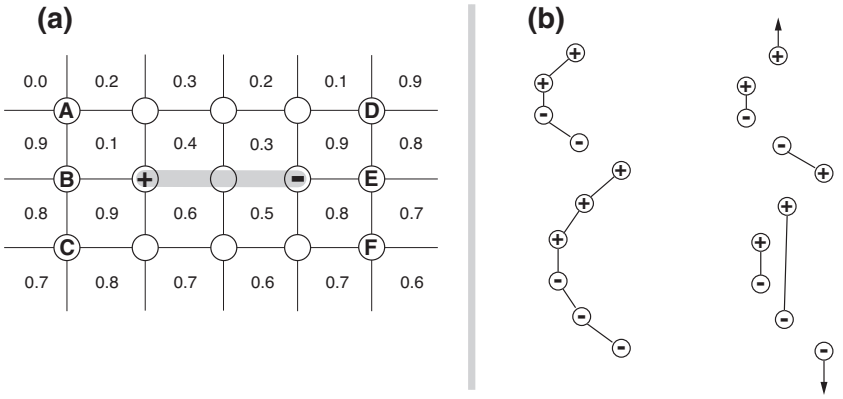


Figure 7.5 (a) The numbers represent a 2-D array of normalized wrapped phase. Summation of the wrapped phase gradient around loops should be zero unless there is a + or – residue. Any phase gradient integration that passes between these two residues will have an unwrapping error, so they are connected by a branch cut (gray line). (b) Two ways to connect residues will result in different unwrapping results. Adapted from Chen and Zebker (2000) with permission from the ©Optical Society of America.

line connecting the two residues is called a *branch cut*. If a negative residue is connected to a positive residue, the two residues are concealed, and no further branch cuts are needed. If both residues were positive, then the branch cut would need to be extended to include two negative residues or neutralized by extending to the edge of the image.

The Goldstein algorithm (Goldstein et al., 1988) first analyzes the wrapped phase to identify all the residues. Then the branch cuts are grown in a tree-like manner such that every residue is on a neutral tree where a tree is a set of connected branch cuts. A branch cut can also extend to the edge of the image where it is neutralized. The phase gradient integration path is not allowed to cross any cuts, so no path includes an unbalanced residue.

As shown in Figure 7.5, there are a variety of ways the residues can be connected. The Goldstein algorithm makes the connections by attempting to minimize the overall length of the branch cuts in an image. One deficiency in the Goldstein algorithm is that branch cuts may be connected in a way to enclose a region in the interferogram so when the path-filling integral is performed, these regions will retain their original wrapped phase.

7.4 Minimum Cost Flow (SNAPHU) Algorithm

The minimum cost flow (MCF) algorithm, as implemented in the SNAPHU program (Chen and Zebker, 2002), also begins with identifying all the residues in

Downloaded from https://www.cambridge.org/core. UNIVERSIDAD AUTONOMA METROPOLITANA, on 13 Nov 2026 at 03:08:40, subject to the Cambridge Core terms of use, available at https://www.cambridge.org/core/terms. https://doi.org/10.1017/9781009606226.008

the image. However, it differs in the way the residues are connected. For both algorithms, the unwrapped phase is identical to the original wrapped phase when re-wrapped. The MCF algorithm attempts to minimize the total number of phase gradient cycles added to the original image.

The MCF algorithm has two variants depending on whether the phase unwrapping is optimal for recovering topography in moderate baseline interferograms or surface deformation in small baseline interferograms. In both cases, the trees are connected in a way that tree branches never cross (i.e., minimum spanning tree), so the phase is unwrapped everywhere. Different interferogram applications may benefit from different objective functions. For example, interferograms for refining topography that are dominated by errors caused by layover differ from interferograms associated with surface ruptures.

An example of the unwrapped phase for the Ridgecrest earthquakes is shown in Figure 7.6. These data were first filtered with a 120-m wavelength Gaussian filter followed by a Goldstein filter. The phase was unwrapped using the SNAPHU algorithm with the discontinuity option set to 60 radians. Unwrapped phase was converted to LOS displacement using Equation 7.1. Figure 7.6 (a), in radar coordinates, matches the wrapped phase shown in Figure 7.1 (a). The integration path from **a** to **b** is largely free of residues, so the surface offset can be measured. Note many areas along the rupture where there are small discontinuous zones. These are mostly phase unwrapping errors. These areas should be masked using a coherence

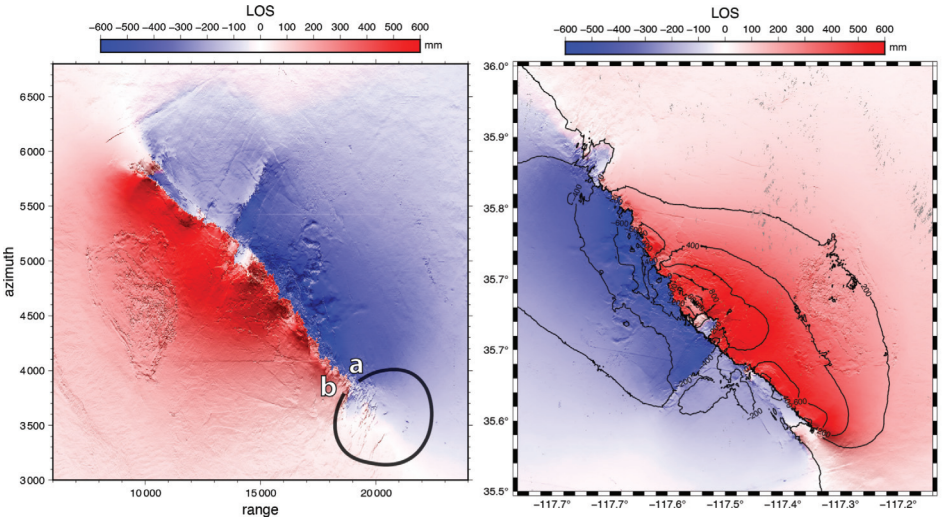


Figure 7.6 (a) LOS deformation in radar coordinates for the Ridgecrest earthquakes. There are many small unwrapping errors along the main ruptures. (b) Same LOS map in geographic coordinates with a 200-mm contour interval shows a maximum LOS offset of more than 1.6 m.

Downloaded from https://www.cambridge.org/core. UNIVERSIDAD AUTONOMA METROPOLITANA, on 13 Nov 2026 at 03:08:40, subject to the Cambridge Core terms of use, available at https://www.cambridge.org/core/terms. https://doi.org/10.1017/9781009606226.008

threshold (Figure 7.1 (b)) or masked manually using the fault trace mapped by geologists after the earthquakes. The right LOS image is in geographic coordinates. The red/blue regions show motion toward/away from the radar, so the NW-SE trending rupture has right-lateral motion while the smaller orthogonal rupture has left-lateral motion as expected.

7.5 Nearest-Neighbor Algorithm and Loop Closure

The SNAPHU algorithm attempts to unwrap the phase everywere including bodies of water where the phase is completely decorrelated. Unwrapping of decorrelated areas dramatically increases the computer time and also introduces phase errors. There are two approaches to minimizing unwrapping errors and computer time. First, areas of noisy phase (e.g., water and coherence < 0.1) could be set to zero, which dramatically speeds the unwrapping. However, this can produce unwrapping errors in nearby areas having high coherence. Consider an interferogram in a coastal area (Figure 7.7). To speed the unwrapping, one resets the phase over the ocean to zero. Next suppose the phase on the land has a ramp parallel to the coastline. The phase unwrapping on the land will attempt to recover this coastline-parallel ramp. However, the phase unwrapping in the ocean will attempt to recover zero phase. There will be a large discontinuity at the coastline, so the MCF algorithm may resolve the conflict by introducing a phase unwrapping error over the land and/or ocean. Of course, the unwrapping error over the land will need to be corrected.

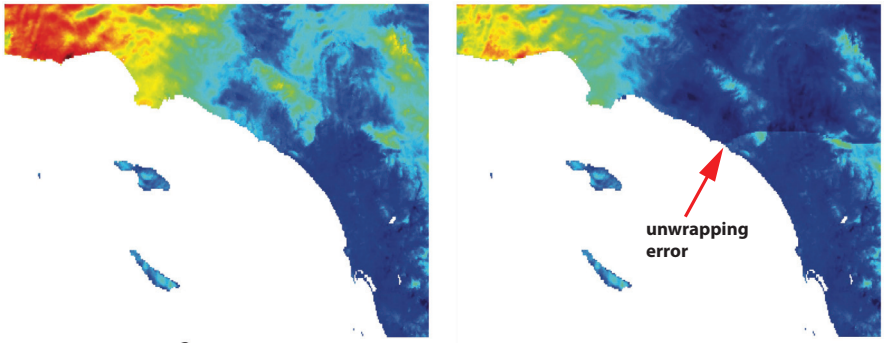


Figure 7.7 Unwrapped phase for Sentinel-1 track 071 covering Southern California in radar coordinates. The area includes Los Angeles, San Diego, and the coastal waters. (a) The phase was unwrapped after setting the water areas to zero phase. This causes an unwrapping error shown by the red arrow. (b) The phase was unwrapped after setting water areas to the phase at the nearest land area. There is no coastal unwrapping error.

Downloaded from https://www.cambridge.org/core. UNIVERSIDAD AUTONOMA METROPOLITANA, on 13 Nov 2026 at 03:08:40, subject to the Cambridge Core terms of use, available at https://www.cambridge.org/core/terms. https://doi.org/10.1017/9781009606226.008

The problem is that the phase over the ocean is completely wrong. Even if the ocean phase was not replaced by zero, this land unwrapping error could still occur because the random ocean phase will unwrap toward zero. To avoid this conflict, Shanker and Zebker (2009) and Lindsey et al. (2014) recommend filling the phase in the water areas with the wrapped value at the closest coastline using a *near-neighbor algorithm*. This approach corrects the phase unwrapping error over the land and dramatically speeds the unwrapping over the ocean. Of course, the unwrapped phase over the ocean will be inaccurate, so it will need to be masked.

The second approach to minimize unwrapping errors, or at least identify the errors, is to use a phase closure constraint when multiple interferograms are available. This is also called 3-D phase unwrapping since the constraint is applied over the time dimension. Consider three SAR images, A, B, and C, that are well correlated. One can construct three interferograms (i.e., phase difference maps) ϕ_{BA}, ϕ_{CB}, and ϕ_{AC}. Of course, the sum of the wrapped phase from these three interferograms should be zero. (Note there can be a small misclosure due to multilooking (Zheng et al., 2022)). After unwrapping these three interferograms, the sum of the phase will not necessarily be zero because of the unknown constant of integration. If each interferogram has no unwrapping errors, then one expects that the sum of the three unwrapped interferograms will be a constant of $N2\pi$ over the entire area. Note that the phase closure can be forced to zero by adding this constant to any of the three interferograms. Suppose further that one of the interferograms has a small area with an unwrapping error of, say, 4π. After the global correction, the sum of the interferograms will be 4π over that small area and zero everywhere else. Using this approach, one can identify the region where the unwrapping error occurred but not necessarily which interferogram has the unwrapping error.

Next consider the case where there are hundreds of interferograms (Figure 7.8). These interferograms will have $N2\pi$ integer ambiguities after the phase is unwrapped. If not properly corrected, this ambiguity term will affect every pixel in radar acquisitions and introduce a random walk-type error that will bias the time series. The use of the phase closure constraint to solve for $N2\pi$ integer ambiguities in unwrapped interferograms is common practice in InSAR time series analysis (e.g., Hussain et al. (2016)). The approach is to form all possible three-way loops in a set of interferograms so the problem can be written into the form of a minimization problem with integer unknowns (Fattahi, 2015). An example is shown in Figure 7.8 using 468 Sentinel-1 interferograms (Xu and Sandwell, 2019). Before solving for the ambiguities, there were typically 300 out of 1 207 loop misclosures in well-correlated areas. After solving for the ambiguities, there were less than 20 misclosures out of 1 207 in the well-correlated areas. Note that in the poorly correlated areas, the number of misclosures remains high 300–400 out of 1 200, so this type of analysis is also good at identifying areas with unreliable results. These areas

Downloaded from https://www.cambridge.org/core. UNIVERSIDAD AUTONOMA METROPOLITANA, on 13 Nov 2026 at 03:08:40, subject to the Cambridge Core terms of use, available at https://www.cambridge.org/core/terms. https://doi.org/10.1017/9781009606226.008

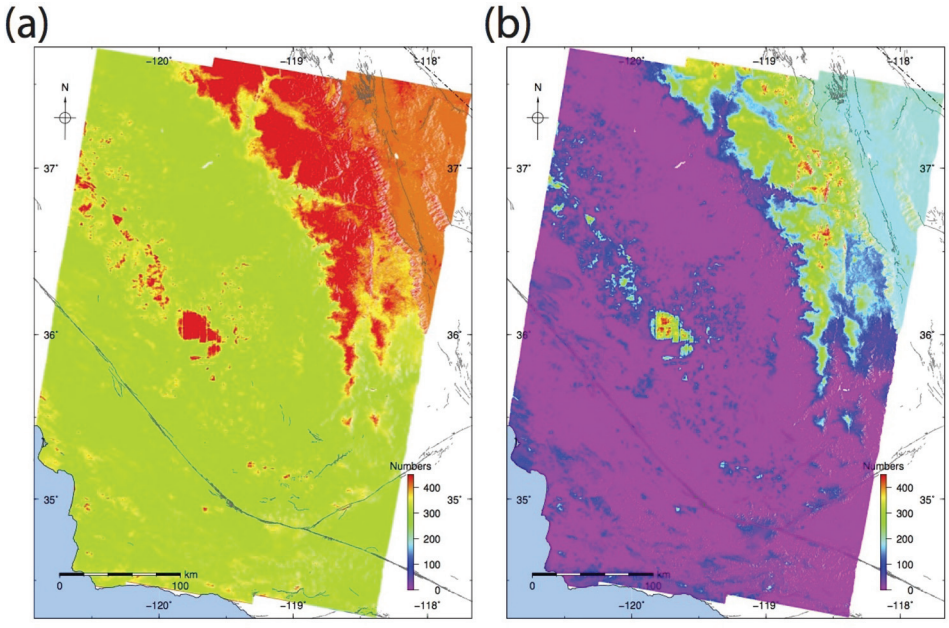


Figure 7.8 (a) Number of nonclosing loops for each pixel before applying the unwrapping ambiguity correction for 81 Sentinel-1 scenes over California (468 interferograms and 1 207 loops). (b) Number of nonclosing loops after correction. Reprinted with permission from *IEEE Transactions on Geoscience and Remote Sensing*.

of high phase misclosure should also be masked or assigned larger uncertainties in any further analysis, such as stacking or time series.

7.6 Summary

Phase unwrapping is one of the most challenging and computing-intensive aspects of radar interferometry. The concept is simple. One selects a starting point in the image and integrates the phase gradient outward to fill the scene with unwrapped phase. If the path encounters a phase jump of greater than π or less than $-\pi$, the algorithm subtracts or adds 2π to recompute the gradient. For noise-free wrapped phase data with no discontinuities, all integration paths between any two points in the image have the same phase offset. This implies that integration around any closed path will have zero phase offset. Because real interferograms are noisy and have phase discontinuities due to layover, shadowing, and surface ruptures, there are points in the interferogram (residues) where closed path integration is either 2π or -2π.

Downloaded from https://www.cambridge.org/core. UNIVERSIDAD AUTONOMA METROPOLITANA, on 13 Nov 2026 at 03:08:40, subject to the Cambridge Core terms of use, available at https://www.cambridge.org/core/terms. https://doi.org/10.1017/9781009606226.008

The global unwrapping approach uses a least squares algorithm to remove, or downweight, the residues and solve for the global unwrapped phase. These global algorithms usually suffer from large-scale errors. Moreover, when the total phase is re-wrapped, the results no longer match the original unwrapped phase.

Local path-following algorithms are usually more successful. The basic approach is to first identify all the residues by summing phase differences around all 2×2 cells in the wrapped phase image. Once these residues are found by thresholding, the algorithms connect them with branch cuts so the sum of the residues along the branch cut is zero. The selection of branch cuts and their assembly into trees is nonunique.

The Goldstein algorithm attempts to minimize the total length of the branch cuts. However, branch cuts can close on themselves, so large areas of the interferogram may be isolated from the path integration and remain unwrapped. One can place the starting point of integration inside this isolated area, but there is an unknown $N2\pi$ ambiguity between the unwrapped phase inside the area and outside the area. Given additional information such as GNSS measurements, one could solve for the $N2\pi$ ambiguity.

The MCF flow algorithm, as implemented in the SNAPHU computer code (Chen and Zebker, 2001), selects the branch cuts to minimize the total number of cycles added to the phase gradient. The branch cuts are connected such that when the growing tree becomes neutral, the next nearest charge is connected to the nearest branch to form a minimum spanning tree. An important property of this tree is that it never closes on itself so every point in the interferogram is connected to every other point and the path-filling integral will unwrap everywhere. Like the Goldstein approach, when this unwrapped phase is re-wrapped, it exactly matches the original unwrapped interferogram.

Just because the unwrapping is complete, it is not necessarily correct. Bodies of water, where phase recovery is impossible, takes an enormous amount of computer time and can produce phase unwrapping on land near the coastlines. To reduce these unwrapping errors, Shanker and Zebker (2009) recommend filling the phase in the water areas with the wrapped value at the closest coastline using a near-neighbor algorithm. This approach dramatically speeds up the unwrapping, including the water areas, but also allows for an accurate phase change along the coastlines.

Phase unwrapping errors can be identified when three or more SAR acquisitions are available for an area. For three SAR images, one can form three interferograms and unwrap their phase. The sum of the three interferograms should have a constant ambiguity of $N2\pi$ everywhere. If part of the summed interferogram has a different ambiguity, then at least one of the three interferograms has a phase unwrapping error. With the hundreds of SAR images available today from missions such as

Downloaded from https://www.cambridge.org/core. UNIVERSIDAD AUTONOMA METROPOLITANA, on 13 Nov 2026 at 03:08:40, subject to the Cambridge Core terms of use, available at https://www.cambridge.org/core/terms. https://doi.org/10.1017/9781009606226.008

Sentinel-1, one can construct and unwrap thousands of interferograms. The summation of unwrapped phase around closed loops will reveal both local and global phase ambiguities. A minimum norm algorithm can be used to approximately solve for the global ambiguities. The remaining local ambiguities reveal areas where there are significant unwrapping errors distributed throughout the interferograms. These high-ambiguity areas can be masked and not used in quantitative analyses.

Later in Chapter 11 we will discuss the use of continuous GNSS measurements to check the global ambiguities and bring the LOS deformation maps into an absolute system. Of course, these InSAR observations are still contaminated with atmospheric delays. After correcting the global ambiguities, the set of interferograms can be used to construct LOS time series. This is also discussed in Chapter 11.

7.7 Problems

1. Write a function in your favorite language/tool to create a sine wave that ranges in amplitude between -2π and 2π over one wavelength and display the image. Then create a wrapped version using atan2() or arctan2(). Then either manually or automatically, unwrap the wrapped version by adding 2π to selected intervals. Hint: Calculate the difference between adjacent pixels going from left to right. If the difference is larger than π, subtract 2π from the remaining series. If the difference is less than $-\pi$, add 2π.
2. Repeat exercise 1 but add 10% noise to the wrapped version and then try unwrapping.
3. Calculate the residue for nodes C, D, E, and F in Figure 7.5.

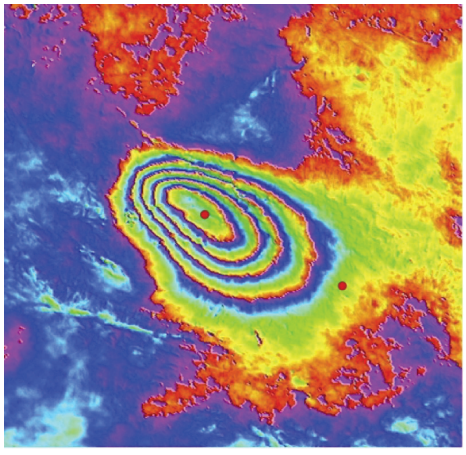


Figure 7.9 A phase change image for the 2017 Sefid Sang M 6.1 earthquake in Iran. This image is from Sentinel-1 data for a descending track.

Downloaded from https://www.cambridge.org/core. UNIVERSIDAD AUTONOMA METROPOLITANA, on 13 Nov 2026 at 03:08:40, subject to the Cambridge Core terms of use, available at https://www.cambridge.org/core/terms. https://doi.org/10.1017/9781009606226.008

4. Why is it 4π instead of 2π in Equation 7.1 converting phase change to displacement?
5. Figure 7.9 is an example of a wrapped phase change for the 2017 Sefid Sang M 6.1 earthquake in Iran. The data is from a descending track of Sentinel-1. How much LOS displacement has occurred between the two red points in Figure 7.9? Is the center of the pattern moving toward or away from the radar?

Downloaded from https://www.cambridge.org/core. UNIVERSIDAD AUTONOMA METROPOLITANA, on 13 Nov 2026 at 03:08:40, subject to the Cambridge Core terms of use, available at https://www.cambridge.org/core/terms. https://doi.org/10.1017/9781009606226.008